Structure, Vol. 12, 1257–1268, July, 2004, ©2004 Elsevier Ltd. All rights reserved. DOI 10.1016/j.str.2004.04.017

The Solution Structure of Type III Effector Protein AvrPto Reveals Conformational and Dynamic Features Important for Plant Pathogenesis

Jennifer Wulf,[1,5] Pete E. Pascuzzi,[1,3,5] Amr Fahmy,[4] Gregory B. Martin,[2,3] and Linda K. Nicholson[1,*]

[1]Department of Molecular Biology and Genetics
[2]Department of Plant Pathology
Cornell University
Ithaca, New York 14853
[3]Boyce Thompson Institute for Plant Research
Ithaca, New York 14853
[4]Department of Biological Chemistry and Molecular Pharmacology
Harvard Medical School
Boston, Massachusetts 02115

Summary

***Pseudomonas syringae* pv. *tomato*, the causative agent of bacterial speck disease of tomato, uses a type III secretion system (TTSS) to deliver effector proteins into the host cell. In resistant plants, the bacterial effector protein AvrPto physically interacts with the host Pto kinase and elicits antibacterial defense responses. In susceptible plants, which lack the Pto kinase, AvrPto acts as a virulence factor to promote bacterial growth. The solution structure of AvrPto reveals a functional core consisting of a three-helix bundle motif flanked by disordered N- and C-terminal tails. Residues required for Pto binding lie in a 19 residue Ω loop. Modeling suggests a hydrophobic patch involving the activation loop of Pto forms a contact surface with the AvrPto Ω loop and that helix packing mediates interactions between AvrPto and putative virulence targets Api2 and Api3. The AvrPto structure has a low stability that may facilitate chaperone-independent secretion by the TTSS.**

Introduction

Many Gram-negative bacterial pathogens of mammals and plants use a type III secretion system (TTSS) to deliver effector proteins (effectors) into the host cell (Galan and Collmer, 1999). Effectors are diverse, and even closely related bacteria express different sets of these proteins (Buttner and Bonas, 2003). One feature common to all effectors is that they are secreted via the TTSS through a long, narrow needle assembly, in some cases requiring assistance from a chaperone (Feldman and Cornelis, 2003; Stebbins and Galan, 2003). In plants, one of the best-studied bacterial pathogens is *Pseudomonas syringae* pv. *tomato*, which causes bacterial speck disease in tomato and *Arabidopsis*. Sequencing of the genome of *P. syringae* pv. *tomato* strain DC3000 revealed the presence of over 30 effectors, significantly more than reported for any bacterial pathogen of mammals (Buell et al., 2003; Fouts et al., 2002). Why plant pathogens express so many effectors is unknown but might relate to the diversity of plant species they attack. The exact role effectors play in the disease process is unknown in most cases, but some effectors encode cysteine proteases, phosphatases, or kinases and probably act by subverting key host defenses (Buttner and Bonas, 2003; Stebbins and Galan, 2001). In support of this hypothesis, host targets of effectors are often critical components of signaling pathways, including protein kinases and Rho GTPases (Shao et al., 2003; Stebbins and Galan, 2000; Wurtele et al., 2001).

The focus of this study is the *P. syringae* pv. *tomato* effector AvrPto, a 164 residue, 18.3 kDa hydrophilic protein with no identifiable homologs in any of the databases (Ronald et al., 1992). Ironically, AvrPto was cloned based on its ability to elicit "gene-for-gene" disease resistance in plants (avirulence) and not for its ability to promote disease (virulence) (Ronald et al., 1992). Resistance in tomato to *P. syringae* pv. *tomato* strains expressing AvrPto is conferred by the Pto R protein, which is a serine/threonine protein kinase (Pedley and Martin, 2003). A direct physical interaction between Pto and AvrPto has been demonstrated in a yeast two-hybrid (Y2H) system, and mutations in either protein that disrupt this interaction also abolish their ability to activate defense in plant cells (Scofield et al., 1996; Tang et al., 1996). This recognition event elicits rapid defense responses in the plant, including the generation of reactive oxygen and nitrogen species, expression of defense-related genes, fortification of cell walls, and a highly localized cell death known as the hypersensitive response (HR) (Martin et al., 2003). Examination of truncated forms of AvrPto has determined that residues 30–125 comprise a minimal region that is sufficient to interact with Pto in yeast (Chang et al., 2001; Tang et al., 1996). Extensive random point mutagenesis of AvrPto has found that residues S94, I96, and G99 are critical for AvrPto binding of Pto (Shan et al., 2000b). The mechanism by which the interaction between AvrPto and Pto triggers the defense response is unknown but does require additional host cell proteins including Prf (Rathjen et al., 1999; Salmeron et al., 1996).

In common with several other effectors, AvrPto also has been shown to enhance pathogen growth and virulence in susceptible plants (Chang et al., 2000; Shan et al., 2000a). Four *Avr*Pto-*i*nteracting (Api) proteins have been isolated from a Y2H screen as possible host targets of AvrPto virulence activity (Bogdanove and Martin, 2000). Api1 is a protein of unknown function but has similarity to a *Phaseolus vulgaris* stress-induced protein. Api4 is an N-myristoyl-transferase and might be responsible for the myristoylation of AvrPto that is believed to occur in the plant cell (Shan et al., 2000b). Api2 and Api3 are putative small GTPases, and both have sequence similarity to human Rab8 and yeast Sec4p proteins (Bogdanove and Martin, 2000). Rab8 and Sec4p are key regulators of protein transport from the Golgi to the plasma membrane (Zahraoui et al., 1989). Intriguingly, AvrPto has recently been shown to suppress the cell wall-based defenses involving papillae formation and to inhibit the

*Correspondence: lkn2@cornell.edu
[5]These authors contributed equally to this work.

expression of genes for secreted proteins (Hauck et al., 2003). A direct physical interaction between AvrPto and the Rab GTPases Api2 and/or Api3 might be a critical determinant for these events. Small GTPases are known to be important virulence targets of effectors expressed by some bacterial pathogens of mammals (Galan and Collmer, 1999).

AvrPto has emerged as a focal point for understanding the molecular mechanisms underlying both virulence and avirulence in a model pathogen-plant system. After secretion through the narrow channel of the TTSS needle, AvrPto is myristoylated and localized to the plasma membrane where it mediates both disease and immunity via interactions with multiple host proteins. Here we present the functional characterization and high-resolution solution structure of a 13 kDa, 105 residue truncated form of AvrPto (TrAvrPto) comprised of residues 29–133. This protein contains the structured core region of AvrPto but lacks the highly mobile N-terminal and C-terminal regions. TrAvrPto binds Pto, Api2, and Api3 in Y2H assays and can elicit Pto-mediated immunity in plants when a minimal myristoylation sequence is restored to the N terminus. These studies provide novel insights into mechanisms of secretion and of interactions with Pto, Api2, and Api3.

Results

AvrPto Contains Disordered N- and C-Terminal Tails

AvrPto was expressed and purified from *E. coli* with a C-terminal FLAG affinity tag (Wulf et al., 2002), which was not cleaved from NMR samples. The two-dimensional (2D) ^{1}H-^{15}N HSQC spectrum of full-length uniformly ^{15}N-labeled AvrPto shows evidence of both ordered and disordered residues (Figure 1A). Mobile, solvent-exposed residues give rise to narrow, intense peaks that cluster toward the center of the spectrum, while residues in ordered regions of structure give rise to broader, less intense peaks dispersed over a wider spectral range. A distinct set of peaks near the center of the spectrum exhibits intensities 15-fold greater than for a second distinct, more disperse set. The intense peaks were assigned via 3D ^{15}N-NOESY and TOCSY data to residues from either the N- or C-terminal regions, indicating AvrPto possesses flexible terminal tails. The expression vector was modified to produce a protein with the same overall charge as full-length AvrPto but lacking the flexible tails (residues 1–28 and 134–164). The N-terminal region is required for TTSS secretion (Lloyd et al., 2001; Anderson et al., 1999) and myristoylation-mediated localization (Shan et al., 2000b), while the role of the C-terminal region in the tomato host is not yet clear. Tail removal dramatically reduced spectral overlap (Figure 1B) and allowed structure determination and functional characterization of the folded core of AvrPto, hereafter designated TrAvrPto. Backbone and side chain assignments for TrAvrPto have been deposited (BioMagResBank code 5311). The structure determination process yielded more complete resonance assignments than were initially reported (Wulf et al., 2002).

TrAvrPto Retains Pto Binding Activity

TrAvrPto was expected to retain Pto binding activity because a truncated form of AvrPto comprised of residues 31–124 was shown to bind Pto in yeast (Chang et al., 2001). This was confirmed by Y2H assays using a TrAvrPto bait fusion and a Pto prey fusion. Both AvrPto and TrAvrPto bind to Pto with similar affinity, as judged by both LEU2 (Figure 1C) and LacZ reporter activity (data not shown). The same TrAvrPto bait fusion also binds Api2 and Api3 prey fusions (data not shown). These results demonstrate that the AvrPto binding functions with avirulence partner Pto and putative virulence targets Api2 and Api3 are preserved in TrAvrPto. Interestingly, the Y2H interaction with Api1 is lost upon deletion of residues 1–28 of AvrPto (data not shown), suggesting a possible virulence function for this region.

TrAvrPto Elicits Pto-Mediated Immunity When Properly Localized in the Plant Cell

When coexpressed in leaves of *N. benthamiana* using an *Agrobacterium*-mediated transient expression system, AvrPto and Pto cause an HR, which is easily assayed (Scofield et al., 1996). Functional analysis of TrAvrPto by this method is complicated by the fact that AvrPto contains an N-terminal myristoylation motif. A G2A point mutation of this motif prevents myristoylation, abolishes plasma membrane localization, and eliminates the avirulence activity of AvrPto (Shan et al., 2000b). Therefore, a minimal myristoylation motif (Utsumi et al., 2001) comprised of the first 9 residues of AvrPto (MGNICVGGS) was fused to TrAvrPto to make MTrAvrPto. G2A point mutants of both AvrPto and MTrAvrPto were included as negative controls. A C-terminal FLAG tag was fused to all constructs to ascertain if it influences AvrPto function. All constructs were subcloned into a plant binary vector, transformed into *Agrobacterium*, and pressure infiltrated into leaves of *N. benthamiana* (Figure 1D).

Both AvrPto and MTrAvrPto cause an HR when coexpressed with Pto. As expected, the G2A mutation abolishes the HR in both AvrPto and MTrAvrPto, because the proteins can no longer be properly localized to the plasma membrane. Likewise, TrAvrPto does not elicit an HR because it lacks the myristoylation motif entirely. The FLAG tag has no apparent effect on AvrPto activity in the plant because it is indistinguishable from the untagged protein in this assay (data not shown). These results define a minimal region of AvrPto sufficient for avirulence activity in the plant cell and confirm that the FLAG tag does not interfere with AvrPto activity, validating the use of TrAvrPto:FLAG for structural studies.

Both AvrPto and TrAvrPto Exhibit a Dynamic Fold with Low Stability and Rapid Exchange between Monomer and Dimer

NMR observations demonstrate that TrAvrPto has a small difference in standard Gibbs free energy (ΔG°_{FU}) between the folded and unfolded states. In addition to the major population of peaks corresponding to folded TrAvrPto, a minor population is evident in the TrAvrPto ^{1}H-^{15}N HSQC spectrum at low contour levels (Figures 1E and 1F). Chemical shifts for this minor population reflect random coil values, indicating that this state is

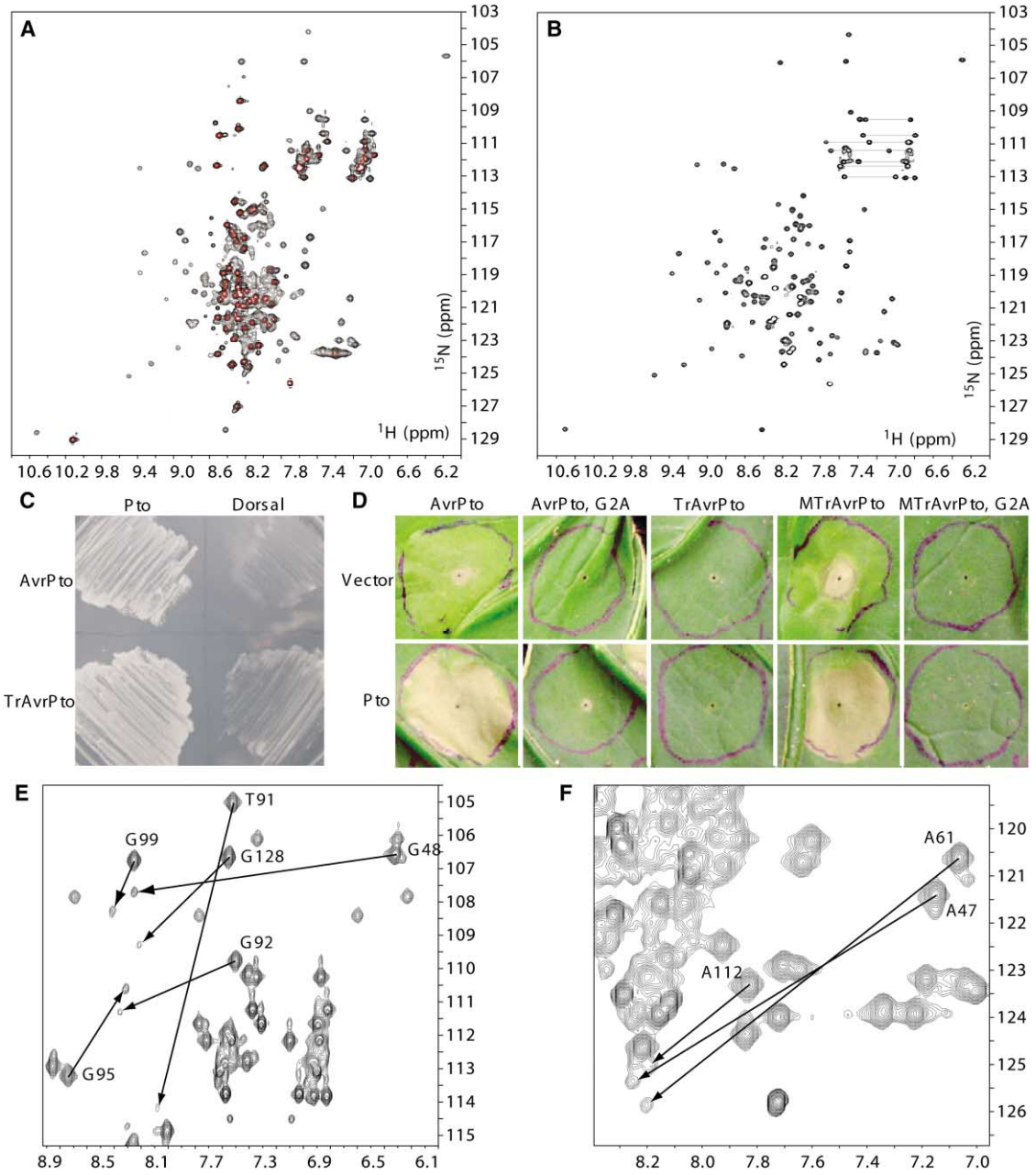

Figure 1. Initial Characterization of AvrPto and TrAvrPto

(A) ^{1}H-^{15}N HSQC spectrum of full-length AvrPto. Peaks corresponding to mobile N- and C-terminal regions are shown in red.

(B) Spectrum of TrAvrPto.

(C) A TrAvrPto bait fusion interacts with a Pto prey fusion in a Y2H assay. Shown is growth on plates lacking leucine under inducing conditions. A dorsal prey fusion was included as a negative control.

(D) TrAvrPto:FLAG causes an HR in plants when the AvrPto minimal myristoylation motif is restored to the N terminus (MTrAvrPto). Leaves of *N. benthamiana* infiltrated with *Agrobacterium* are shown for each coexpression experiment. Photos were taken at 4 dpi.

(E) An unfolded population is evident in ^{1}H-^{15}N-HSQC spectrum at low contour levels. Peaks of five glycine residues and T91 are well dispersed in the major population, indicating ordered structure. Corresponding peaks in the minor population are shifted toward random coil positions.

(F) Peaks of A47, A61, and A112 exhibit similar behavior as those in (E), indicating that the minor population represents a global, unfolded state.

unstructured. Resolved peaks from the unfolded population were assigned to residues throughout the TrAvrPto protein via sequential NOEs and d_{NN} exchange peaks with their counterparts in the folded population. The observation of d_{NN}s between amide ^{1}Hs in the two states provides sufficient proof that conformational exchange between folded and unfolded forms occurs at a rate that is slow relative to the chemical shift time scale (ca. 300 s^{-1}). The ratio of folded/unfolded TrAvrPto populations determined from peak volumes for nine resolved,

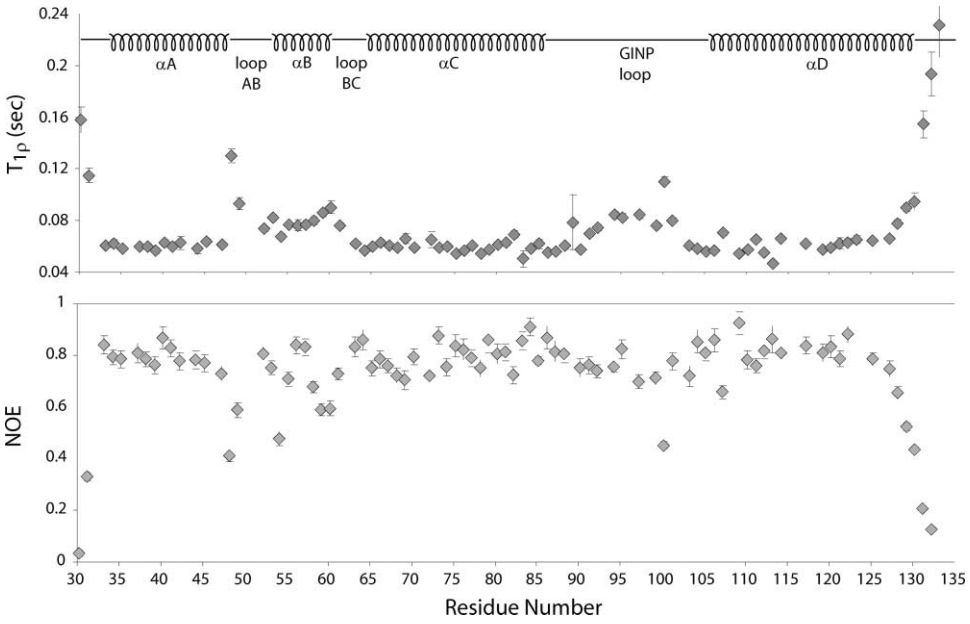

Figure 2. Backbone Dynamics Parameters of TrAvrPto

Transverse relaxation ($T_{1\rho}$) and steady-state heteronuclear $^{15}N\{^1H\}$-NOE values for backbone NHs are plotted versus residue number. These parameters are sensitive indicators of backbone flexibility on the picosecond to nanosecond time scale. Low $^{15}N\{^1H\}$-NOE coupled with high $T_{1\rho}$ values indicate high mobility. The average $T_{1\rho}$ for ordered residues (0.060 ± 0.006 s) is consistent with a dimer.

assigned peaks was 9:1 (±5), corresponding to $\Delta G^{\circ}_{FU} \approx -1.3$ kcal/mol for a system at thermal equilibrium. The corresponding population ratio for full-length AvrPto was 2:1 (±1) ($\Delta G^{\circ}_{FU} \approx -0.4$ kcal/mol), indicating an even lower stability for the full-length protein. The FLAG tag had no significant effect on protein stability because similar results were obtained when the FLAG tag was removed from TrAvrPto (data not shown).

Native gel electrophoresis and Y2H data suggest that AvrPto and TrAvrPto each exist as dimers (P.E.P. and G.B.M., unpublished data). NMR data and dynamic light scattering (DLS) measurements are also consistent with a dimer in solution. Relaxation measurements indicate slower global tumbling than expected for a monomer (Figure 2), with the T_1/T_2 ratio for NH bonds across the backbone indicating a range of effective correlation times consistent with anisotropic tumbling of a 26 kDa dimer (data not shown). AvrPto molecular weight (MW) was estimated by DLS for an AvrPto NMR sample (1.0 mM) and for subsequent serial dilutions (0.5, 0.3, and 0.2 mM). The resulting MWs were all within experimental error of 38 kDa, approximately twice the monomeric AvrPto MW (inclusive of the C-terminal FLAG tag).

To evaluate the effect of TrAvrPto dimerization on the interpretation of NOEs used in structure calculations, isotope-filtered NMR experiments designed to transfer magnetization from protons on labeled to unlabeled nuclei were used (Zwahlen et al., 1997). No intermolecular cross peaks were observed even after denaturation/refolding (confirmed by ^{15}N-^1H HSQC), indicating that the dimer lifetime is insufficient for observable cross-relaxation across the interface. The T76 hydroxyl proton, observable due to hydrogen bonding, provided an internal control since it is not bonded to ^{13}C. The same cross peaks (including long-range) to $T76^{OH}$ were observed in the filtering experiments (both before and after denaturation/refolding) as in non-isotope-filtered NOESY spectra (where cross peaks to $T76^{OH}$ are weaker than the average across each spectrum), confirming effective transfer. Thus, the observed NOEs reflect the average structure of a single subunit, and all observed distance restraints were applied to the monomer structure.

From the above analysis, TrAvrPto exists in dynamic equilibrium between folded and unfolded ensembles in which the dominant form is a folded dimer. Monomer and dimer states interconvert within the folded ensemble, while exchange between the folded and unfolded ensembles also occurs.

TrAvrPto Molecular Architecture

A final ensemble of 50 structures was calculated, and the 30 lowest energy structures were included in the final ensemble analysis (Table 1). The atomic root-mean-square deviation (rmsd) about the mean for residues 33–83 and 103–128 is 0.45 ± 0.07 Å for backbone and 0.95 ± 0.1 Å for all heavy atoms (Figure 3A). The rmsd for the entire construct, inclusive of the flexible termini (residues 29–32 and 129–133) and a long, internal loop (residues 84–102), is 0.97 ± 0.2 Å for the backbone and 1.32 ± 0.2 Å for all heavy atoms. Coordinates for the ensemble have been deposited at the Protein Data Bank (accession code 1R5E).

TrAvrPto consists of three long helices (αA, αC, and αD) arranged in an antiparallel left-hand twisted bundle, one short perpendicular helix (αB) flanked by two short loops (loops AB and BC), and one long loop between αC and αD (loop CD). The compact cylindrical protein measures approximately 50 Å along its long axis with a 25 Å diameter. Loop CD is denoted the GINP loop based on a putative sequence motif conserved between *P.*

Table 1. Structural Statistics

Restraints Used in Structure Calculations		
	Initial	Final
Distance Restraints		
Intraresidue	328	784
Sequential	360	389
Medium range	161	225
Long range	37	186
Hydrogen bond	0	108
Dihedral restraints		
ϕ, φ	103,103	103,103
Total restraints per residue	10.4	18.1
Geometric Statistics		
Rmsd from idealized geometry		
Bonds (Å)	0.0012 ± 0.0001	
Angles (°)	0.31 ± 0.01	
Improper (°)	0.15 ± 0.01	
Ramachandran Analysis	Residues Evaluated	
	33–83, 102–128	29–133
Most favored regions (%)	91.1	82.0
Additionally allowed regions (%)	8.7	17.6
Generously allowed regions (%)	0.1	0.4
Disallowed regions (%)	0	0
Equivalent resolution (backbone, Å)	1.0	2.1
Equivalent resolution (hydrogen bond energy, Å)	2.4	2.2
Dihedral G factor	−0.03	−0.44
Lennard-Jones Potential Energies[a]	Av (kcal/mol)	Std. Dev.
Total	−1490.5	53.6
Bond	2.5	0.2
Angle	42.1	1.3
Improper	3.0	.03
Electric	−1538.1	53.7

[a] For 30 lowest energy structures.

syringae effectors AvrPto and AvrPtoB that appears to be required for Pto recognition of AvrPto (Kim et al., 2002; Shan et al., 2000a) (Figure 3B). The isolated loop displays an ensemble backbone rmsd of 1.1 ± 0.6 Å; this significant ordering is not an artifact of energy minimization, because removal of loop restraints significantly increases this rmsd to 3.6 ± 0.7 Å. Four defined turns are present: a type III β-like turn (R88-T91) and three inverse γ turns (Q86-R88, G92-S94, and N97-G99). An additional 90° kink is centered at G95. The resulting broad head region of the loop is twisted ~90° relative to the base. The most solvent exposed GINP loop residues are Y89, P98, and R88. Residue R88 forms a "lid" over the center of the loop, while Y89 protrudes upward into solvent (Figure 3C). High mobility is evident only at the extreme N- and C-terminal ends and at G48 and M100 (Figure 2).

A striking feature of the structure is the long GINP Ω loop, which contains key residues required for interaction with Pto (Shan et al., 2000b). This loop displays hallmark features of an Ω loop, with no repeating elements of α helix or β strand and terminal residues D84 and P102 within 10 Å of each other and less than 2/3 the maximum Cα-Cα distance between loop residues (19.6 Å) (Leszczynski and Rose, 1986). However, atypical amino acids are present, most notably three Mets, one Ile, and one Leu (Fetrow, 1995). Ω loops often contain residues critical for function, and the presence of these atypical and predominantly hydrophobic residues in the solvent-exposed GINP loop suggests particular importance of these residues in AvrPto function.

TrAvrPto Shares Structural Homology with Other Proteins

Although sequence homologs have yet to be identified, the fold of AvrPto is not unique. A search using the refined TrAvrPto structure and the Vector Alignment Search Tool (VAST) (Madej et al., 1995) revealed six structural homologs (Table 2; Figure 4). The three structures with the most striking similarity to AvrPto are the α-helical region of the substrate binding domain of the molecular chaperone, DnaK (Zhu et al., 1996), the three-helix bundle domain of the Golgi α-mannosidase II (van den Elsen et al., 2001), and the de novo designed protein model of radical enzymes (Dai et al., 2002) (Figure 4). The pair-wise backbone heavy-atom rmsd for TrAvrPto with DnaK, α-mannosidase II, and the radical enzyme model are 1.5, 1.4, and 1.5 Å, respectively, for the regions that structurally align (indicated in Figure 4A in uppercase lettering). Interestingly, H471 of α-mannosidase is involved in the coordination of a catalytic zinc ion and overlays onto a putative copper(I) binding site in TrAvrPto. In TrAvrPto, the copper binding consensus sequence M_{82}-xx-M_{85}-x-H_{87}-xx-M_{90} (Cha and Cooksey,

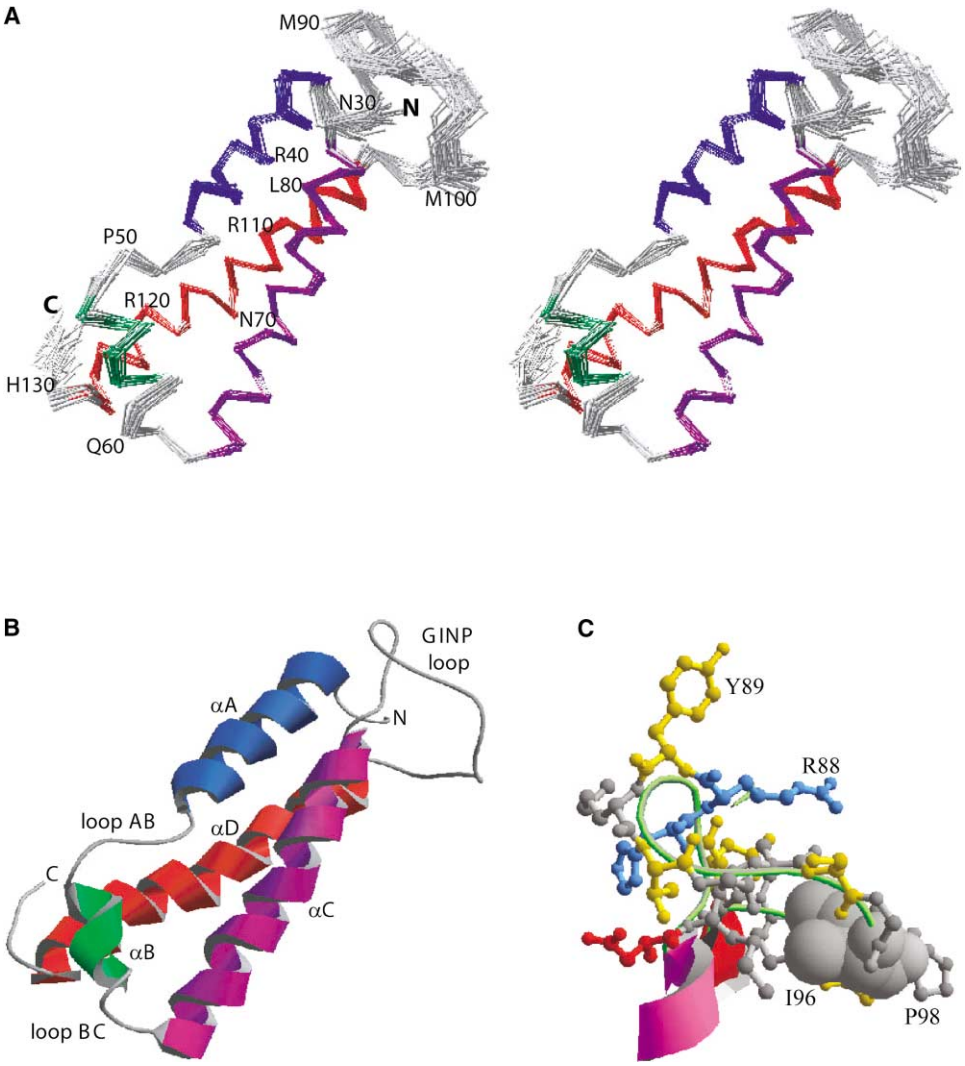

Figure 3. Structure of TrAvrPto

(A) Stereoview of 25 overlaid low-energy structures. Helices are colored blue (αA, S33–S46), green (αB, D52–S59), purple (αC, N70–A83), and red (αD, H103–G128).

(B) Ribbon diagram of TrAvrPto for the minimized average of the 50 final structures (coloring as in [A]).

(C) Detail of the GINP loop (residues D84–P102). R88 forms a "lid" over the center of the loop, while Y89 protrudes upward into solvent.

1991) lies at the end of αC and the start of the GINP loop. The physical significance of this putative copper binding site and its relevance to function are currently under investigation.

The GINP Ω Loop Mediates Interactions with Pto

Saturation random mutagenesis of AvrPto has identified 12 residues that are believed to be important for AvrPto binding to Pto (Chang et al., 2001; Shan et al., 2000b). Of these, 11 fall within TrAvrPto. The TrAvrPto structure reveals that the substitutions made at seven of these residues (L43, S46, D52, L65, L72, Q86, and N105) are likely to destabilize the fold, suggesting that these side chains do not directly bind to Pto. Residues L43, L65, and L72 are buried in the hydrophobic core, whereas S46, D52, Q86, and N105 form interactions that require

Table 2. Structural Homologues of TrAvrPto

Protein	% Aligned		PDB#
	Residues	Sequence	
Substrate binding domain of the molecular chaperone DnaK	60%	10%	1DKZ
Drosophila Golgi α-mannosidase II	59%	6%	1HTY
De novo designed protein model of radical enzyme	51%	3%	1LQ7
Staphylococcal protein A	31%	3%	1BDC
E. coli MsbA	30%	10%	1JSQ
Reovirus membrane-penetration protein m1	30%	9%	1JMU

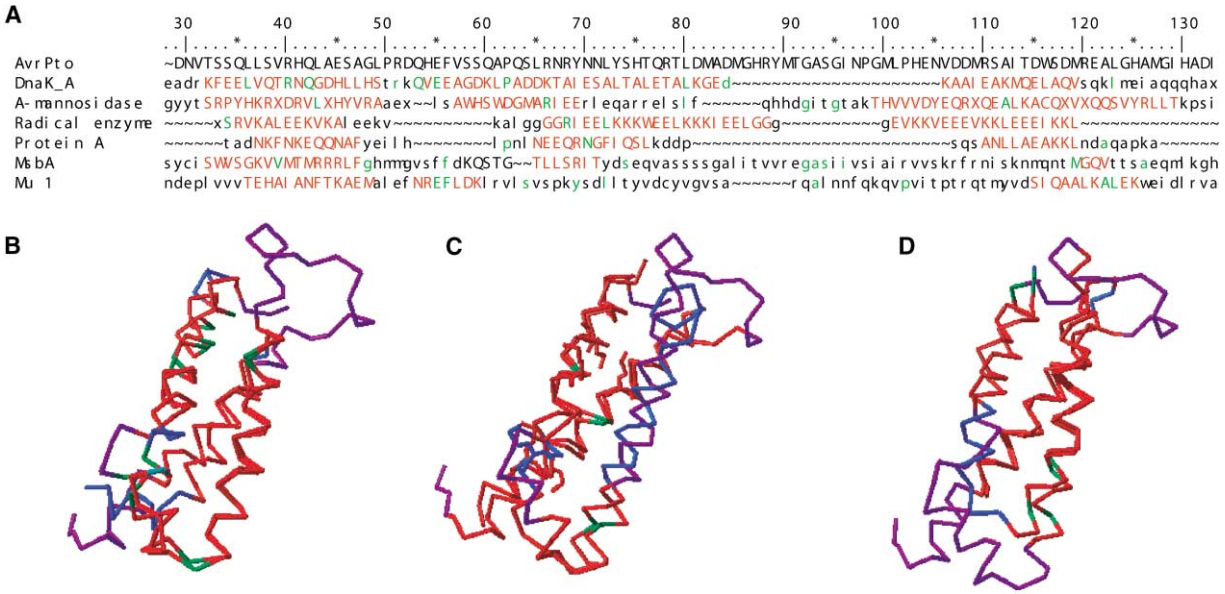

Figure 4. Structural Homologs of TrAvrPto

(A) Sequence alignments (numbering corresponds to AvrPto). Regions of both structure and sequence identity (green), structural alignment only (red), and sequence identity only (green lower case) are indicated. Cα trace overlays of TrAvrPto (purple) with structural homologs (blue) from (B) DnaK, (C) the Golgi α-mannosidase II, and (D) the de novo designed radical enzyme. Regions of structural alignment (red) and sequence identity (green) are indicated.

the geometry and chemical features of the native side chains. The remaining four residues occur in the GINP loop (Figure 5A). To determine if the isolated GINP loop sequence is sufficient to interact with Pto in yeast, an oligomer coding for residues D84–P102 was cloned into plasmid pJG4-5 to make a Y2H prey fusion (Golemis, 1996). In this construct, the GINP loop is not anchored at its C terminus as it is in AvrPto. Protein expression was confirmed by Western blotting; however, no interaction between the GINP loop prey and a Pto bait fusion was detected (data not shown). A full-length AvrPto prey was included as a positive control. Therefore, both the primary sequence and the tertiary structure of the GINP loop appear to be important for Pto binding in yeast.

The nonconservative GINP loop mutations, Q86P/R, S94P, I96T, and G99V, all abolish the AvrPto-Pto interac-

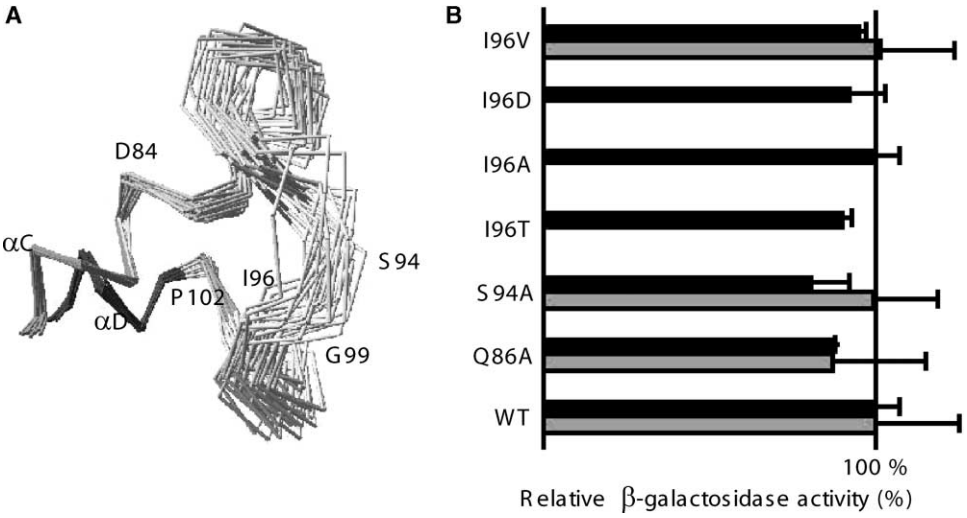

Figure 5. The GINP Ω Loop of AvrPto Is a Critical Structural Determinant for Pto Binding

(A) Overlay of 25 low-energy structures shows that the GINP loop is well ordered.

(B) Residues in the GINP loop are critical for interaction with Pto. Point mutations of GINP loop residues were made in AvrPto, and the interaction with Pto (gray bars) was tested by Y2H assays. An Api1 prey (black bars) provides a positive control to demonstrate protein expression and localization. AvrPto interacts more strongly with Pto than with Api1. Therefore, the percentage values plotted reflect the measured units normalized with respect to wild-type AvrPto. Even conservative mutations at I96 (I96A) abolish the interaction with Pto but do not affect the interaction with Api1.

tion in Y2H assays (Chang et al., 2001; Shan et al., 2000b). To further define the structural determinants required for interaction with Pto, additional GINP loop mutations were made and analyzed by quantitative Y2H assays (Figure 5B). All tested mutants interact with Api1 with near normal affinity, demonstrating proper protein expression and nuclear localization for the AvrPto bait fusions. Wild-type behavior of Q86A and S94A demonstrates that these side chains are not critical for the interaction. Rather, these results suggest the requirement for a specific backbone conformation, a conclusion supported by the previously reported Q86P/R, S94P, and G99V loss-of-function mutants. In the GINP Ω loop structure, both S94 and G99 are the third residue in an inverse γ turn; the S94 NH hydrogen bonds to the carbonyl of G92, while G99 adopts torsion angles attainable only by glycine. Hence, in agreement with the Y2H results for the GINP loop peptide described above, the Ω loop conformation is critical for the AvrPto-Pto interaction.

Mutations at I96 show that a hydrophobic side chain at this position is particularly important for the interaction with Pto. Substitution with a polar (I96T), charged (I96D), or neutral (I96A) amino acid abolishes the interaction with Pto. Only the I96V mutant behaves as wild-type. This result suggests that AvrPto may interact with a hydrophobic surface of Pto.

Discussion

Structural Homology Suggests that AvrPto Has Evolved for Multiple Interactions

Although TrAvrPto and its structural homologs have no direct functional similarity, the compact three-helix bundle conformation they share provides a stable, versatile, and efficient subunit that is used primarily for recognition and binding. In DnaK, two faces of its three-sided helical bundle interact with a β sandwich subdomain (Zhu et al., 1996), whereas the third face may be the binding site for the regulatory cochaperone DnaJ (Wasryzynow et al., 1995). In α-mannosidase, the small α-helical domain forms extensive tertiary contacts that maintain the relative orientations of two larger domains (van den Elsen et al., 2001). It is clear that the helical bundle of AvrPto is well suited for mediating multiple binding interactions with host proteins, including Pto, Api2, and Api3.

Implications of Low ΔG°_{FU} for AvrPto Secretion and Binding

There is evidence that the TTSS exports proteins in an unfolded or partially folded state, because the channel they must pass through is estimated to be only $\sim$2 nm in diameter (Cordes et al., 2003). Fusion of effectors to ubiquitin, a highly stable protein of $\sim$2.5 nm diameter that resists unfolding, prevents their secretion (Lee and Schneewind, 2002). Destabilization of the ubiquitin fold with specific point mutations restores the secretion of the effector fusions (Lee and Schneewind, 2002). For some effectors, their cognate chaperones serve to maintain them in partially unfolded states (Feldman and Cornelis, 2003; Stebbins and Galan, 2003). There are no reports that AvrPto ($\sim$2.5 nm diameter) requires a chaperone for secretion. Our findings indicate that AvrPto has an inherently low ΔG°_{FU} and maintains a significant population of unfolded protein. This low stability could be a general feature of some effectors that would allow for chaperone-independent secretion (Feldman and Cornelis, 2003). This low stability would also allow for posttranslational secretion with a protein-based secretion signal (Lloyd et al., 2001) but is also fully consistent with cotranslational secretion utilizing a mRNA signal (Anderson et al., 1999). Our NMR studies of TrAvrPto provide the first evidence that a bacterial effector possesses inherently low stability and suggests a direct relationship between protein folding and secretion via the TTSS.

The low stability of AvrPto also has important implications for modulating its interactions with host proteins. As has been postulated for other systems (Plaxco and Gross, 2001; Ramelot et al., 2000; Wright and Dyson, 1999), $\Delta G_{binding}$ can be significantly enhanced when the free energy of one binding partner is high (e.g., it adopts a disordered state). The binding reaction is essentially a final step of folding, in which the interaction surface of the other binding partner provides the required interactions for adopting a stable fold. The low stability of AvrPto would allow a large $\Delta G_{binding}$ without requiring an extensive interaction surface area or extraordinary interaction energies across the binding interface.

Implications of the TrAvrPto Structure for the Mechanism of Interaction with Pto, Api2, and Api3

It is not yet known whether host targets bind to dimeric or monomeric AvrPto. Although the low level of AvrPto in an infected plant cell favors monomer, the effective concentration at the plasma membrane may be sufficient for the dimer to play a functional role. Even so, the AvrPto dimer may be disrupted upon binding to host targets (i.e., the dimer may play a "storage" role, providing protection from proteolysis until a target is encountered). Hence, it is informative to consider implications of the TrAvrPto structure for interactions with host target proteins.

The interaction between AvrPto and the Pto kinase is an important model system for understanding recognition events underlying plant disease resistance. The studies described herein provide a picture of the AvrPto surface involved in Pto recognition. The GINP Ω loop, poised at one end of the helical bundle of AvrPto, provides a partially hydrophobic surface with specific geometrical and chemical features that are recognized by the Pto kinase. How might this loop dock into its recognition surface on Pto? Several Pto point mutants that abolish binding of AvrPto are known (Frederick et al., 1998; Scofield et al., 1996). Interpretation of Pto mutational data is subject to the usual stability concerns and is further complicated by potential effects on kinase activity. However, the transference of AvrPto binding activity to the closely related Fen kinase by a single substitution (N204T) clearly implicates a solvent-exposed surface of Pto in AvrPto binding (Frederick et al., 1998). In addition to T204, other Pto residues are implicated

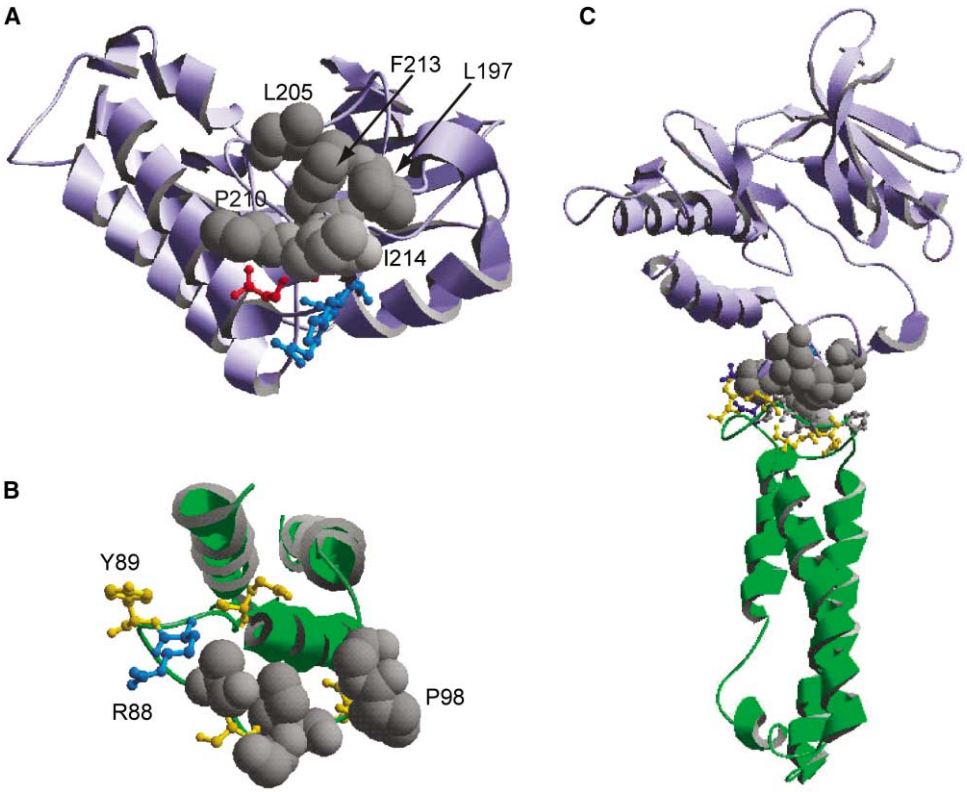

Figure 6. Model for AvrPto/Pto Interaction

Both proteins are shown as ribbon diagrams (Pto in blue, AvrPto in green). Interface residues are shown as space-filled gray (hydrophobic), and ball-and-stick yellow (polar), red (acidic), or blue (basic).

(A) Putative Pto interaction surface.

(B) AvrPto interaction surface.

(C) Model of the AvrPto/Pto complex. The model, obtained using the docking program TreeDock (Fahmy and Wagner, 2002), has the lowest van der Waals interaction energy (−30.921 kcal/mol) among 5×10^4 different orientations of AvrPto and Pto in which P98 C′ and L197 $C^{\delta 2}$ atoms remain in contact. The R88 "lid" was manually swung into an "open" conformation prior to docking.

in AvrPto binding (Rathjen et al., 1999). Among these, substitution of D164 with A, G, or E abolishes binding to AvrPto, while D164N retains binding. Based on a homology model of Pto residues 42–240 (Sessa et al., 2000), T204 is in the C-terminal region of the activation loop and forms an OH...COO^- hydrogen bond with D164. Requirement of this hydrogen bond for interaction with AvrPto is consistent with the mutational data, as it would be disrupted by the D164A/G/E and T204N substitutions but would be retained in the D164N mutant. The D164-T204 hydrogen bond stabilizes the activation loop conformation, in which T204 is adjacent to a hydrophobic patch formed by residues L197, L205, I208, P210, F213, and I214 (Figure 6A).

A potential model for the AvrPto/Pto complex was obtained by docking the GINP loop against the T204-related hydrophobic surface of Pto using the program TreeDock (Fahmy and Wagner, 2002). In this model, AvrPto binds with its long axis perpendicular to the Pto surface (Figure 6C), and Pto residues L197, T198, L205, I208, D209, P210, E211, F213, I214, K215, R217, and Y225 are within 5 Å of the GINP loop. The model, although based on monomeric TrAvrPto, is also compatible with numerous possible dimer forms. Relative to the canonical kinase catalytic core structure, helix αG and its connecting loops (not present in the Pto homology model) would be displaced by AvrPto binding, suggesting that a novel switch mechanism might be involved in AvrPto regulation of Pto kinase activity. This proposed model will allow the prediction and testing of additional critical residues for AvrPto's role in eliciting host immunity. From the perspective of host resistance, the high-resolution TrAvrPto structure represents a significant advancement toward understanding how the binding of AvrPto to Pto activates signaling pathways leading to host immunity.

The TrAvrPto structure yields additional insights into the mode of binding to the GTPase homologs Api2 and Api3 (Api2/3), which are putative virulence targets of AvrPto. Several effectors from bacterial pathogens of animals are known to target GTPases (Galan and Collmer, 1999). The recently determined structures of ExoS and SptP bound to Rac1 show that these effectors have adapted—through convergent evolution using the four-helix bundle as a scaffold—a binding surface on the side of the bundle that mimics the host GAP domains and packs against the GTPase (Stebbins and Galan, 2000; Wurtele et al., 2001). Structural similarity of these effectors with the three-helix bundle core of AvrPto suggests similar helix side packing as a possible mecha-

nism for AvrPto interactions with Api2/3. The structurally diverse GTPase effector proteins also commonly utilize helix packing at the GTPase binding interface (Ostermeier and Brunger, 1999). Mutations of AvrPto that abolish Pto binding and avirulence, while still enhancing virulence, suggest that different structural regions of AvrPto mediate interactions with Pto and Api2/3 (Shan et al., 2000a). A GTPase binding surface formed by the side of the TrAvrPto helical bundle would be distinct from the Pto binding surface model presented above. Various models for how AvrPto interacts with Api2/3 can now be tested through site-directed mutagenesis and subsequent Y2H analyses. Resulting loss-of-binding mutants will provide powerful tools for probing the significance of Api2/3 as virulence targets of AvrPto.

The solution structure of TrAvrPto represents an important step toward understanding the mechanisms behind this unique protein's opposing roles in eliciting host resistance and enhancing pathogen virulence. The versatility of AvrPto is derived from a compact three-helix bundle and a large Ω loop that form its structured core. The three-helix bundle allows multiple, nonexclusive binding surfaces, as exemplified by structurally homologous domains found in DnaK and α-mannosidase. Previously, there was no understanding of the structural mechanisms by which AvrPto interacts with host proteins. Our high-resolution TrAvrPto structure, coupled with synergistic mutational and functional analyses, now enables the physical basis for these interactions to be visualized.

Experimental Procedures

Mutagenesis and Plasmid and Strain Construction

Site-directed mutagenesis of AvrPto was performed in plasmid pFLAG-CTC (Sigma, St. Louis, MO) using the Quickchange protocol and *Pfu* Turbo DNA polymerase (Stratagene, La Jolla, CA). Mutagenesis was confirmed by complete sequencing of the AvrPto inserts. For protein expression, the pFLAG-CTC AvrPto was introduced into *E. coli* BL21 Gold cells using the provided protocol (Stratagene).

Yeast Two-Hybrid Assays

Bait fusions of AvrPto in pNLexA (Golemis, 1996) were made by PCR-amplifying AvrPto clones from the pFLAG constructs described above. The 5′ primer introduced an EcoRI site and a Kozak consensus sequence for efficient translation, while the 3′ primer contained a XhoI site. The sequence of all bait fusions was confirmed by sequencing. Yeast strain EGY48 was used, and all yeast transformations and assays for LEU2 and LacZ reporter activity were performed using standard methods (Golemis, 1996).

Agrobacterium-Mediated Transient Expression

AvrPto clones for transient assays were prepared as above, except a plant Kozak sequence was incorporated. All constructs were subcloned into the KpnI and XbaI sites of the binary vector pBTEX (provided by R. Bressan, Purdue University, West Lafayette, IN). Plasmids were introduced into *Agrobacterium* strain GV2260 by electroporation. Cells were grown overnight in LB media supplemented with rifampicin (10 mg/l) and kanamycin (25 mg/l) to an OD_{600} of 2–3. Cells were washed twice with 10 mM MES (pH 5.5) containing 200 μM acetosyringone (Aldrich), and the appropriate strains were mixed for coexpression and resuspended to a final OD_{600} of 0.14 for infiltration. The leaves of approximately 8-week-old *N. benthamiana* plants were infiltrated with cell suspensions with a needle-less 1 ml syringe.

NMR Sample Preparation

The expression, purification, and $^{15}N/^{13}C$ labeling of C-terminal FLAG-tagged full-length AvrPto and TrAvrPto have been previously reported (Wulf et al., 2002). TrAvrPto consists of AvrPto residues 29–133, an N-terminal Met, a C-terminal Val, and the 8 residue FLAG peptide. Protein concentrations were determined by UV spectroscopy at 280 nm using calculated extinction coefficients of 17,780 $M^{-1}cm^{-1}$ for AvrPto and 10,810 $M^{-1}cm^{-1}$ for TrAvrPto (Gill and von Hippel, 1989). Uniformly labeled samples were concentrated to ca. 1 mM in AvrPto buffer (10 mM Na_2HPO_4, 5 mM KH_2PO_4, 225 mM NaCl, 10 mM DTT [omitted for TrAvrPto], 0.02% NaN_3 [pH 6.0]).

NMR Spectroscopy

All NMR experiments were performed at 25°C on a Varian Inova 600 MHz spectrometer equipped with an {H,C,N} probe equipped with a self-shielded pulsed-field gradient. Proton chemical shifts were referenced relative to external DSS (1 mM [pH 6.0], 25°C) and were used to calculate the absolute zero frequencies of ^{13}C and ^{15}N (Cavanagh et al., 1996). In most cases, data were apodized using a phase-shifted sine-bell function and zero-filled prior to Fourier transformation. For data sets recorded with a limited number of points in indirectly detected dimension(s), linear prediction was used. Spectra were processed with NMRPipe/NMRDraw (Delaglio et al., 1995) and analyzed with PIPP (Garret et al., 1991).

Experimental Restraints

Distance restraints were obtained from assigned crosspeaks in 3D ^1H-^{15}N NOESY-HSQC, 3D ^1H-^{13}C NOESY-HSQC (in H_2O and D_2O), as well as 2D and 3D ^1H-^{13}C NOESY-HSQC spectra optimized for aromatics. Interresidue NOEs were categorized by intensity, and upper distance restraints for each category were set to 2.8 (short), 3.6 (medium), 4.5 (long), and 5.3 (very long) Å. Dihedral angle restraints were obtained using TALOS (Ψ and ϕ) (Cornilescu et al., 1999) and confirmed using a 3D HNHA spectrum (ϕ only). Hydrogen bond restraints were inferred from regions of stable 2° structure and the absence of solvent exchange.

To investigate intermolecular NOEs across the dimer interface, isotope-filtered experiments were performed (Zwahlen et al., 1997). A 2D ^{13}C F_1-filtered, F_3-edited NOESY-HSQC experiment (mix = 100 ms) was first performed using a 1:1 mixture of uniformly $^{13}C/^{15}N$-labeled/unlabeled TrAvrPto prepared by combining molar equivalents of 1.0 mM separately prepared $^{13}C/^{15}N$-labeled and natural abundance samples of TrAvrPto. The sample was then lyophilized twice and resuspended in D_2O. Aliphatic and aromatic 2D versions were collected (mix = 100 and 200 ms). A 3D ^{13}C F_1-filtered, F_3-edited NOESY-HSQC spectrum was collected (mix = 100 ms). The protein was then denatured by diluting to 0.02 mM in AvrPto buffer with the addition of 8 M urea, and refolded by slow dialysis against reduced concentrations of urea (4, 2, 1, and then 0 M). The sample was then concentrated, and the experiments were repeated as above.

Structure Calculations

The iterative torsion angle dynamics/simulated annealing protocol of CNS was used (Brunger et al., 1998). Default parameters were used with the exception that the first torsion slow-cool annealing stage was extended to 60,000 steps and followed by a 10,000-step Cartesian slow-cool annealing stage. Initially, ten-structure ensembles were calculated using only CαCβ chemical shifts, and dihedral angle and unambiguous NOE restraints. These were used to manually correct and uniquely identify any additional NOE assignments used in subsequent structure calculations. The quality of resulting structures was checked using AQUA and PROCHECK-NMR (Laskowski et al., 1996). Structures were visually analyzed with SwissPdb Viewer (Guex and Peitsch, 1997). Refinement continued until no additional NOEs could be assigned and the resulting structures contained no significant violations. CαCβ restraints were removed when there were no longer dihedral violations $>5°$. Hydrogen bond restraints for helices were added as helical regions became well defined and backbone rmsd reached 2.0 Å. Hydrogen bond acceptors for $G48^{HN}$ and $T76^{OH}$ were identified by visual inspection of the ensembles when backbone rmsd reached 0.8 Å. The final 30 lowest energy structures had no violations exceeding the following: 0.16 Å (NOE), 0.04 Å (hydrogen bond), and 2° (dihedral).

Relaxation

Backbone ^{1}H-^{15}N NOE, and ^{15}N T_1 and $T_{1\rho}$ measurements were performed, processed, and analyzed as described previously (Wang et al., 2001). T_1 decay was sampled at nine different time points: 0.011, 0.088, 0.165, 0.242, 0.330, 0.495, and 0.661 s; time points at 0.011 and 0.661 s were sampled twice. $T_{1\rho}$ decay was sampled at nine different time points: 0.008, 0.016, 0.024, 0.032, 0.048, 0.064, and 0.096 s; time points at 0.008 and 0.096 s were sampled twice.

Dynamic Light Scattering

A DynaPro MSTC Dynamic Light Scattering Instrument (Protein Solutions) was used. DLS measurements were made for serial dilutions of 1:0, 1:1, 1:2, and 1:4 of a 1.0 mM NMR sample (diluted with NMR buffer). The theoretical MW for each sample was calculated using standard DynaPro software.

Acknowledgments

We would like to thank Rob Abramovitch, Jeff Anderson, and Anjali Iyer for critical reading of this manuscript, Martha Schloot Field and Norma Pawley for assistance with dynamics analyses, and Kevin Tan for experimental assistance. This research was supported by the Park Foundation, the Triad Foundation, the Boyce Thompson Institute for Plant Research, United States Department of Agriculture NRI grant no. 02-35301-12020 (G.M.), NSF grant no. MCB-0212597 (L.K.N.), NSF grant no. DBI-0077622 (G.M.), NIH grant GM47467 (A.F.), and a NSF Graduate Research Fellowship (P.E.P.).

Received: February 29, 2004
Revised: April 28, 2004
Accepted: April 28, 2004
Published: July 13, 2004

References

Anderson, D.M., Fouts, D.E., Collmer, A., and Schneewind, O. (1999). Reciprocal secretion of proteins by the bacterial type III machines of plant and animal pathogens suggests universal recognition of mRNA targeting signals. Proc. Natl. Acad. Sci. USA *96*, 12839–12843.

Bogdanove, A.J., and Martin, G.B. (2000). AvrPto-dependent Pto-interacting proteins and AvrPto-interacting proteins in tomato. Proc. Natl. Acad. Sci. USA *97*, 8836–8840.

Brunger, A.T., Adams, P.D., Clore, G.M., Delano, W.L., Gros, P., Grosse-Kunstleve, R.W., Jiang, J.-S., Kuszewski, J., Nilges, N., Pannu, N.S., et al. (1998). Crystallography and NMR system: a new software suite for macromolecular structure determination. Acta Crystallogr. *D54*, 905–921.

Buell, C.R., Joardar, V., Lindeberg, M., Selengut, J., Paulsen, I.T., Gwinn, M.L., Dodson, R.J., Deboy, R.T., Durkin, A.S., Kolonay, J.F., et al. (2003). The complete genome sequence of the *Arabidopsis* and tomato pathogen *Pseudomonas syringae* pv. *tomato* DC3000. Proc. Natl. Acad. Sci. USA *100*, 10181–10186.

Buttner, D., and Bonas, U. (2003). Common infection strategies of plant and animal pathogenic bacteria. Curr. Opin. Plant Biol. *6*, 312–319.

Cavanagh, J., Fairbrother, W.J., Palmer, A.G.I., and Skelton, N.J. (1996). Protein NMR Spectroscopy: Principles and Practice (New York: Academic Press).

Cha, J.-S., and Cooksey, D.A. (1991). Copper resistance in *Pseudomonas syringae* mediated by periplasmic and outer membrane proteins. Proc. Natl. Acad. Sci. USA *88*, 8915–8919.

Chang, J.H., Rathjen, J.P., Bernal, A.J., Staskawicz, B.J., and Michelmore, R.W. (2000). *avrPto* enhances growth and necrosis caused by *Pseudomonas syringae* pv. *tomato* in tomato lines lacking either *Pto* or *Prf*. Mol. Plant Microbe Interact. *13*, 568–571.

Chang, J.H., Tobias, C.M., Staskawicz, B.J., and Michelmore, R.W. (2001). Functional studies of the bacterial avirulence protein AvrPto by mutational analysis. Mol. Plant Microbe Interact. *14*, 451–459.

Cordes, F.S., Komoriya, K., Larquet, E., Yang, S., Egelman, E.H., Blocker, A., and Lea, S.M. (2003). Helical structure of the needle of the type III secretion system of *Shigella flexneri*. J. Biol. Chem. *278*, 17103–17107.

Cornilescu, G., Delaglio, F., and Bax, A. (1999). Protein backbone angle restraints from searching a database for chemical shift and sequence homolgy. J. Biomol. NMR *13*, 289–302.

Dai, Q.-H., Tommas, C., Fuentes, E.J., Blomberg, M.R.A., Dutton, P.L., and Wand, A.J. (2002). Structure of a *de novo* designed protein model of radical enzymes. J. Am. Chem. Soc. *124*, 10952–10953.

Delaglio, F., Grzesiek, S., Vuister, G.W., Zhu, G., Pfeifer, J., and Bax, A. (1995). NMRPipe: a multidimensional spectral processing system based on UNIX Pipes. J. Biomol. NMR *6*, 277–293.

Fahmy, A., and Wagner, G. (2002). TreeDock: a tool for protein docking based on minimizing van der Waals energies. J. Am. Chem. Soc. *124*, 1241–1250.

Feldman, M.F., and Cornelis, G.R. (2003). The multitalented type III chaperones: all you can do with 15 kDa. FEMS Microbiol. Lett. *219*, 151–158.

Fetrow, J.S. (1995). Omega loops: nonregular secondary structures significant in protein function and stability. FASEB J. *9*, 708–717.

Fouts, D.E., Abramovitch, R.B., Alfano, J.R., Baldo, A.M., Buell, C.R., Cartinhour, S., Chatterjee, A.K., D'Ascenzo, M., Gwinn, M.L., Lazarowitz, S.G., et al. (2002). Genomewide identification of *Pseudomonas syringae* pv. *tomato* DC3000 promoters controlled by the HrpL alternative sigma factor. Proc. Natl. Acad. Sci. USA *99*, 2275–2280.

Frederick, R.D., Thilmony, R.L., Sessa, G., and Martin, G.B. (1998). Recognition specificity for the bacterial avirulence protein AvrPto is determined by Thr-204 in the activation loop of the tomato Pto kinase. Mol. Cell *2*, 241–245.

Galan, J.E., and Collmer, A. (1999). Type III secretion machines: bacterial devices for protein delivery into host cells. Science *284*, 1322–1328.

Garret, D.S., Powers, R., Gronenborn, A.M., and Clore, G.M. (1991). A common sense approach to peak picking in two-, three-, and four-dimensional spectra using automatic computer analysis of contour diagrams. J. Magn. Reson. *95*, 214–220.

Gill, S.C., and von Hippel, P.H. (1989). Calculation of protein extinction coefficients from amino acid sequence data. Anal. Biochem. *182*, 319–326.

Golemis, E., Gyuris, J., and Brent, R. (1996). Interaction trap/two-hybrid system to identify interacting proteins. In Current Protocols in Molecular Biology, F. Ausubel, R. Brent, R.E. Kingston, D.D. Moore, J.G. Seidman, J.A. Smith, and K. Struhl, eds. (New York: Green and Wiley), pp. 13.14.11–13.14.17.

Guex, N., and Peitsch, M.C. (1997). SWISS-MODEL and the Swiss-Pdb Viewer: an environment for comparative protein modeling. Electrophoresis *18*, 2714–2723.

Hauck, P., Thilmony, R.L., and He, S.Y. (2003). A *Pseudomonas syringae* type III effector suppresses cell wall-based extracellular defense in susceptible *Arabidopsis* plants. Proc. Natl. Acad. Sci. USA *100*, 8577–8582.

Kim, Y.J., Lin, N.C., and Martin, G.B. (2002). Two distinct *Pseudomonas* effector proteins interact with the Pto kinase and activate plant immunity. Cell *109*, 589–598.

Laskowski, R.A., Rullmann, J.A.C., MacArthur, M.W., Kaptein, R., and Thornton, J.M. (1996). AQUA and PROCHECK-NMR: programs for checking the quality of protein structures solved by NMR. J. Biomol. NMR *8*, 477–486.

Lee, V.T., and Schneewind, O. (2002). Yop fusions to tightly folded protein domains and their effects on *Yersinia enterocolitica* type III secretion. J. Bacteriol. *184*, 3740–3745.

Leszczynski, J.F., and Rose, G.D. (1986). Loops in globular proteins: a novel category of secondary structure. Science *234*, 849–855.

Lloyd, S.A., Norman, M., Rosqvist, R., and Wolf-Watz, H. (2001). *Yersinia* YopE is targeted for type III secretion by N-terminal, not mRNA, signals. Mol. Microbiol. *39*, 520–531.

Madej, T., Gibrat, J.-F., and Bryant, S.H. (1995). Threading a database of protein cores. Proteins *23*, 356–369.

Martin, G.B., Bogdanove, A.J., and Sessa, G. (2003). Understanding

the functions of plant disease resistance proteins. Annu. Rev. Plant Biol. *54*, 23–61.

Ostermeier, C., and Brunger, A.T. (1999). Structural basis of Rab effector specificity: crystal structure of the small G protein Rab3A complexed with the effector domain of rabphilin-3A. Cell *96*, 363–374.

Pedley, K., and Martin, G.B. (2003). Molecular basis of Pto-mediated resistance to bacterial speck disease in tomato. Annu. Rev. Phytopathol. *41*, 215–243.

Plaxco, K.W., and Gross, M. (2001). Unfolded, yes, but random? Never! Nat. Struct. Biol. *8*, 659–660.

Ramelot, T.A., Gentile, L.N., and Nicholson, L.K. (2000). Transient structure of the amyloid precursor protein cytoplasmic tail indicates preordering of structure for binding to cytosolic factors. Biochemistry *39*, 2714–2725.

Rathjen, J.P., Chang, J.H., Staskawicz, B.J., and Michelmore, R.W. (1999). Constitutively active Pto induces a Prf-dependent hypersensitive response in the absence of AvrPto. EMBO J. *18*, 3232–3240.

Ronald, P., Salmeron, J., Carland, F., and Staskawicz, B. (1992). The cloned avirulence gene *avrPto* induces disease resistance in tomato cultivars containing the *Pto* resistance gene. J. Bacteriol. *174*, 1604–1611.

Salmeron, J.M., Oldroyd, G.E.D., Rommens, C.M.T., Scofield, S.R., Kim, H.-S., Lavelle, D.T., Dahlbeck, D., and Staskawicz, B.J. (1996). Tomato *Prf* is a member of the leucine-rich repeat class of plant disease resistance genes and lies embedded within the *Pto* kinase gene cluster. Cell *86*, 123–133.

Scofield, S.R., Tobias, C.M., Rathjen, J.P., Chang, J.H., Lavelle, D.T., Michelmore, R.W., and Staskawicz, B.J. (1996). Molecular basis of gene-for-gene specificity in bacterial speck disease of tomato. Science *274*, 2063–2065.

Sessa, G., D'Ascenzo, M., and Martin, G.B. (2000). Thr38 and Ser198 are Pto autophosphorylation sites required for the AvrPto-Pto-mediated hypersensitive response. EMBO J. *19*, 2257–2269.

Shan, L., He, P., Zhou, J.-M., and Tang, X. (2000a). A cluster of mutations disrupt the avirulence but not the virulence function of AvrPto. Mol. Plant Microbe Interact. *13*, 592–598.

Shan, L., Thara, V.K., Martin, G.B., Zhou, J.-M., and Tang, X. (2000b). The *Pseudomonas* AvrPto protein is differentially recognized by tomato and tobacco and is localized to the plant plasma membrane. Plant Cell *12*, 2323–2338.

Shao, F., Golstein, C., Ade, J., Stoutemyer, M., Dixon, J.E., and Innes, R.W. (2003). Cleavage of *Arabidopsis* PBS1 by a bacterial type III effector. Science *301*, 1230–1233.

Stebbins, C.E., and Galan, J.E. (2000). Modulation of host signaling by a bacterial mimic: Structure of the *Salmonella* effector SptP bound to Rac1. Mol. Cell *6*, 1449–1460.

Stebbins, C.E., and Galan, J.E. (2001). Structural mimicry in bacterial virulence. Nature *412*, 701–705.

Stebbins, C.E., and Galan, J.E. (2003). Priming virulence factors for delivery into the host. Nat. Rev. Mol. Cell Biol. *4*, 738–743.

Tang, X., Frederick, R.D., Zhou, J., Halterman, D.A., Jia, Y., and Martin, G.B. (1996). Initiation of plant disease resistance by physical interaction of AvrPto and Pto kinase. Science *274*, 2060–2063.

Utsumi, T., Sato, M., Nakano, K., Takemura, D., Iwata, H., and Ishisaka, R. (2001). Amino acid residue penultimate to the amino-terminal Gly residue strongly affects two cotranslational protein modifications, N-myristoylation and N-acetylation. J. Biol. Chem. *276*, 10505–10513.

van den Elsen, J.M.H., Kuntz, D.A., and Rose, D.R. (2001). Structure of the Golgi α-mannosidase II: a target for inhibition of growth and metastasis of cancer cells. EMBO J. *20*, 3008–3017.

Wang, C., Pawley, N.H., and Nicholson, L.K. (2001). The role of backbone motions in ligand binding to the c-Src SH3 domain. J. Mol. Biol. *313*, 873–887.

Wasryzynow, A., Banecki, B., Wall, D., and Liberek, K. (1995). ATP hydrolysis is required for the DnaJ-dependent activation of DnaK chaperone for binding to both native and denatured protein substrates. J. Biol. Chem. *270*, 19307–19311.

Wright, P.E., and Dyson, H.J. (1999). Intrinsically unstructured proteins: re-assessing the protein structure-function paradigm. J. Mol. Biol. *293*, 321–331.

Wulf, J., Pascuzzi, P.E., Martin, G.B., and Nicholson, L.K. (2002). Letter to the editor: ^{1}H, ^{15}N and ^{13}C chemical shift assignments of the structured core of the *Pseudomonas* effector protein AvrPto. J. Biomol. NMR *23*, 247–248.

Wurtele, M., Wolf, E., Pederson, K.J., Buchwald, G., Ahmadian, M.R., Barbieri, J.T., and Wittinghofer, A. (2001). How the *Pseudomonas aeruginosa* ExoS toxin downregulates Rac. Nat. Struct. Biol. *8*, 23–26.

Zahraoui, A., Touchot, N., Chardin, P., and Tavitian, A. (1989). The human Rab genes encode a family of GTP-binding proteins related to yeast YPT1 and SEC4 products involved in secretion. J. Biol. Chem. *264*, 12394–12401.

Zhu, X., Zhao, X., Burkholder, W.F., Gragerov, A., Ogata, C.M., Gottesman, M.E., and Hendrickson, W.A. (1996). Structural analysis of substrate binding by the molecular chaperone DnaK. Science *272*, 1606–1614.

Zwahlen, C., Legault, P., Vincent, S.J.F., Greenblatt, J., Konrat, R., and Kay, L.E. (1997). Methods for measurement of intermolecular NOEs by nuclear NMR spectroscopy: application to a bacteriophage λ N-peptide/*boxB* RNA complex. J. Am. Chem. Soc. *119*, 6711–6721.

Accession Numbers

Coordinates for the ensemble have been deposited at the Protein Data Bank (accession code 1R5E).